Int. J. Solids Structures, 1970, Vol. 6, pp. 1357 to 1376. Pergamon Press. Printed in Great Britain

LIMIT BEHAVIOR OF FIBROUS MATERIALS†

P. V. McLAUGHLIN, JR.

University of Illinois, Urbana, Illinois

and

S. C. BATTERMAN

University of Pennsylvania, Philadelphia, Pennsylvania

Abstract—This paper studies the limit behavior of fibrous materials which are composed of planar arrays of long elastic, perfectly plastic fibers site bonded or imbedded in a strengthless matrix. The upper and lower bound limit theorems are used to obtain equations for limit surfaces of representative structural elements of fibrous membranes in terms of the number, orientation and limit load of the constituent fibers. The effects of fiber orientation geometry, fiber yielding, fiber buckling and pullout of fibers from the remaining structure are included in the theory and illustrated with numerical examples. Experimental results consisting of uniaxial tensile tests of metal wire mats and non-woven fabrics are compared to analytical predictions.

INTRODUCTION

A CLASS of fibrous materials and structures exists which depends almost entirely on the load bearing capacity of the fibers for their strength. Materials such as paper, non-woven fabrics, fibrous metal mats, or metal fiber-reinforced plastics derive their strength from interfiber site bonding with no continuous matrix, or by having the fiber structures imbedded in a matrix which serves only to transfer load and maintain positional geometry but adds no significant strength of its own. It is materials of this nature, that fail by perfectly plastic flow of fibers, elastic buckling of fibers [1, 2] and pullout of fibers from the remaining structure [3] which are investigated in this paper.

It was recently shown [4] that the upper and lower bound limit theorems of plasticity [5] can be extended to include phenomena other than perfectly plastic flow and that fiber buckling and pullout are admissible limit phenomena as long as they occur under constant fiber axial load. Furthermore, it was also shown that structural collapse which occurs due to any combination of acceptable limit phenomena can be handled within the framework of limit analysis. Limit analysis techniques are used in the present paper to develop equations for limit surfaces for representative structural elements of fibrous membranes having arbitrary fiber orientation and density and which exhaust their load carrying capacity due to one or any combination of perfectly plastic flow, constant load buckling, and constant load fiber pullout. It will be shown that not only are these surfaces exact for fibrous

† Based in part on a dissertation submitted to the University of Pennsylvania by P. V. McLaughlin, Jr. in partial fulfillment of the requirements for the degree of Doctor of Philosophy. P. V. McLaughlin, Jr. is grateful for the support of the Scott Paper Company and S. C. Batterman gratefully acknowledges the support of the National Science Foundation and the Advanced Research Projects Agency while making this study.

structures which are site bonded or impregnated with a strengthless matrix, but they are also a rigorous lower bound to the limit surfaces for fibrous structures having a matrix whose strength is not negligible.

Hill [6] has investigated the behavioral laws of a general class of perfectly plastic composites, and has shown, among other things, the existence of extremal surfaces in mean stress space obeying the usual classical normality and convexity relations. These extremal surfaces, which have all the qualities of the classical yield surfaces for perfectly plastic materials, are completely analogous to the limit surfaces developed herein for fibrous composites which can fail by buckling and pullout in addition to plastic flow.

It should be mentioned that Drucker [7] has used limit analysis techniques to determine the strength of a rigid particle suspension in a perfectly plastic matrix under uniaxial tension. Strength of uniaxially fiber reinforced materials has been investigated for several material and geometrical configurations by Hashin [8], Shu and Rosen [9] and Dow *et al.* [10]. Limit analysis was used to determine strength in axial and transverse tension and shear for restricted geometries, notably the composite cylinder assemblage. In all cases, presence of a matrix and contribution of its strength to that of the composite was an important feature of the analysis. A qualitative discussion of how layers of unidirectionally reinforced composite sheets may be stacked to obtain high tensile strength in more than one direction is given by Gerard and Lashmikantham [11], who predict an approximate maximum biaxial strength envelope for symmetrical biaxial reinforcement with and without a matrix. No attempt is made by any of the above authors, however, at obtaining complete yield surfaces for structural elements of fibrous composites.

Shaffer [12] has determined the elastic–plastic stress field in a uniaxially reinforced plastic matrix loaded transversely to the fibers, and Mulhern *et al.* [13] have analyzed a continuum model for single fiber family reinforcement of an elastic–plastic matrix. Both papers are concerned only with elastic fibers, and multi-family plastic fibers are given no consideration. Mechanics of non-woven fabrics has been studied by several workers (see, for example, [3, 14]), where the main effort has been on predicting uniaxial tensile stress–strain characteristics. However, no attempt was made to predict limit surfaces or fabric strength under biaxial tension and shear loading.

In the next section, the limit theorems are used to obtain limit surfaces for membranes composed of multiple families of fibers having arbitrary orientations and number densities, and show the effect of fiber orientation, fiber buckling and fiber pullout. Examples are given to illustrate the theory. Finally, experimental results consisting of uniaxial tensile tests of metal wire mats and non-woven fabrics are compared to analytical predictions.

ANALYSIS

Geometry and equilibrium of a representative structural element

The fibrous membrane material for which limit surfaces will be developed is typified by a representative structural element (RSE) which is composed of many long, nearly straight fibers at various orientations in a plane. All fibers are elastic–perfectly plastic with behavior as illustrated in Fig. 1. The fibers will all be assumed to have identical geometrical and material properties. However, membranes containing any other specific configurations of fibers having different properties (e.g. a membrane composed of both nylon and steel fibers) can also be analyzed by the method outlined herein. There may

or may not be a matrix of another material surrounding the fibers. If there is a matrix, it is assumed to be strengthless insofar as resultant load bearing capacity is concerned, but strong enough to transfer load to fibers and maintain fiber structural geometry. The RSE is small compared to the total structure size, but large compared to the spacing between fibers such that all typical fiber groups are contained in the element. In addition, fibers may be interwoven, but the depth scale of the interweave is assumed very small and flexural effects in the structural element are insignificant compared to membrane force effects.

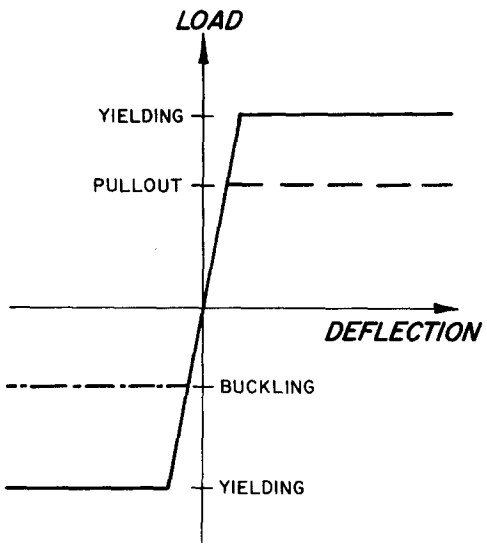

FIG. 1. Load-deflection curve for a single fiber showing ideal plasticity, fiber pullout and fiber buckling.

Define rectangular cartesian axes x and y fixed in the center of the RSE [Fig. 2(a)] which is square and of unit dimensions. An angle θ is defined only between $-\pi/2$ and $\pi/2$ measured positive counterclockwise from the x axis, and gives the orientation of the fibers in the RSE.

The RSE is composed of n families of fibers, each fiber in the ith family having a specific orientation θ_i where $\theta_i > \theta_{i-1}$ and θ_i may be negative [Fig. 2(b)]. There are v_i fibers per unit length perpendicular to the fiber axis in the ith family. It can be shown that the total length of the fibers of the ith family contained in the RSE is also v_i.

If v_i is the length of ith family fibers per unit area of membrane and ρ_l is fiber mass density per unit length, then the total length of all fibers per unit area of membrane, L_f, and the fiber mass per unit area of membrane, M_f, are, respectively,

$$L_f = \sum_{i=1}^{n} v_i \tag{1}$$

$$M_f = \rho_l \sum_{i=1}^{n} v_i. \tag{2}$$

We will be considering RSE's which are undergoing collapse, and hence all or nearly all of the fibers in the RSE will be at their collapse loads. If the fiber spacing for a given family is not uniform in the RSE and fibers have the same load, there will be, in addition to force resultants, an arbitrary number of in-plane force moments of various order. These moments are analogous to multipolar stresses for continua, the simplest of which are couple stresses. Since a discussion of couple or multipolar effects is beyond the scope of

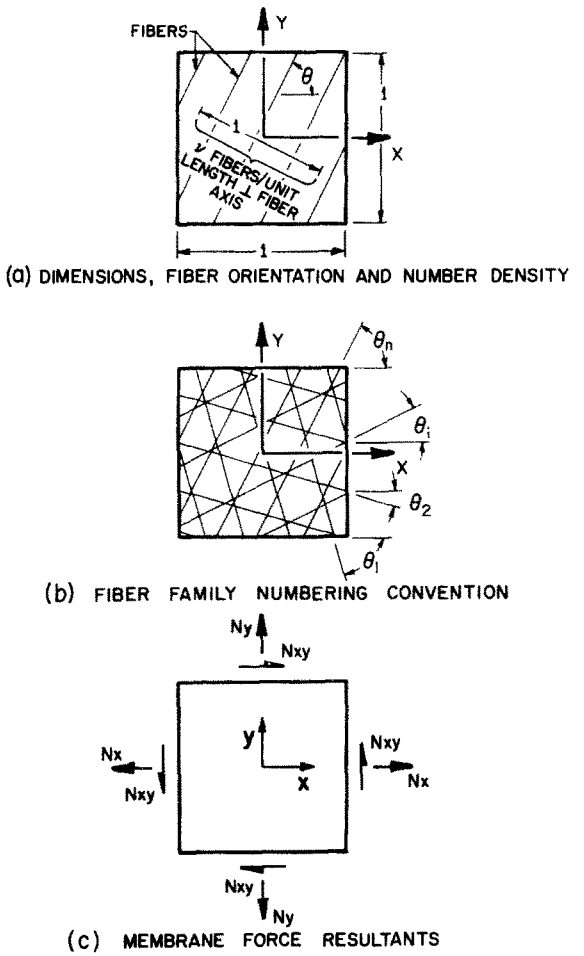

FIG. 2. Representative structural element of fiber membrane.

this paper, we will assume that all fibers in a given ith family are equally spaced and hence the family's number density ν_i is constant in the RSE. Under these conditions, the most general membrane force resultants are normal forces N_x and N_y, and shear forces N_{xy} per unit length [Fig. 2(c)]. If the axial force in each fiber oriented at θ_i is f_i positive in tension and negative in compression, we may write the membrane resultant normal and shear

forces as

$$N_x = \sum_{i=1}^{n} f_i v_i \cos^2 \theta_i$$

$$N_y = \sum_{i=1}^{n} f_i v_i \sin^2 \theta_i \tag{3a, b, c}$$

$$N_{xy} = \sum_{i=1}^{n} f_i v_i \sin \theta_i \cos \theta_i$$

Denote the magnitude of a fiber's limit load in tension by f° and in compression by $\varphi_c f^\circ$. It will be convenient when computing limit surfaces to define the following non-dimensional membrane force

$$n_s = \frac{N_s}{f^\circ \sum_{i=1}^{n} v_i} \tag{4}$$

where the subscript s can be either x, y or xy. It is seen that n_s is the ratio of the actual membrane force under consideration to the maximum tensile membrane force if all fibers were oriented in the direction of pull.

If we let

$$\varphi_i = \frac{f_i}{f^\circ} \tag{5}$$

be the non-dimensional force in fibers which are oriented at angle θ_i, we may rewrite the fiber force–membrane stress equilibrium equations as

$$n_x = \frac{\sum_{i=1}^{n} \varphi_i v_i \cos^2 \theta_i}{\sum_{i=1}^{n} v_i}, \qquad n_y = \frac{\sum_{i=1}^{n} \varphi_i v_i \sin^2 \theta_i}{\sum_{i=1}^{n} v_i},$$

$$n_{xy} = \frac{\sum_{i=1}^{n} \varphi_i v_i \sin \theta_i \cos \theta_i}{\sum_{i=1}^{n} v_i}. \tag{6a, b, c}$$

The general limit surface for a fibrous membrane

The limit surface for a general fibrous membrane which collapses due to any combination of plastic flow, buckling, or pullout of fibers will be obtained by using the limit analysis theorems [4, 5] to compute coincident upper and lower bounds.

To compute an upper bound to the membrane limit surface, assume an RSE collapse mode consisting of the RSE edges or boundaries deforming linearly with their position in the plane. Let the RSE edge velocity be $\mathbf{v}(x, y) = v_x\mathbf{i} + v_y\mathbf{j}$, where x and y are the position coordinates of points on the RSE edges, $\mathbf{i}$ and $\mathbf{j}$ are unit vectors parallel to the x and y axes,

respectively, and the velocity varies linearly with position of the edges:

$$v_x = \dot{\varepsilon}_x x + \dot{\varepsilon}_{xy} y, \qquad v_y = \dot{\varepsilon}_{xy} x + \dot{\varepsilon}_y y. \tag{7a,b}$$

Here, $\dot{\varepsilon}_x$, $\dot{\varepsilon}_y$ and $\dot{\varepsilon}_{xy}$ are constants and represent membrane extensional strain rates and shear strain rate, respectively. Note that the RSE edge and hence only fiber ends are subjected to a linear velocity, and fiber deformation in the interior remains unspecified.

The axial extensional strain rate of any fiber oriented at θ_i is

$$\dot{e}_{a_i} = \dot{\varepsilon}_x \cos^2 \theta_i + \dot{\varepsilon}_y \sin^2 \theta_i + 2\dot{\varepsilon}_{xy} \sin \theta_i \cos \theta_i. \tag{8}$$

It should be noted that if fibers are either buckling or pulling out of the structure $\dot{\varepsilon}_x$, $\dot{\varepsilon}_y$, $\dot{\varepsilon}_{xy}$ and $\dot{e}_{a_i}$ are not strictly strain rates. In these two cases, however, $\dot{\varepsilon}_x$, $\dot{\varepsilon}_y$ and $\dot{\varepsilon}_{xy}$ do represent the relative velocities of the RSE edges in the x and y directions and as such are valid deformation measures in the limit analysis sense [4]. Similarly, even though $\dot{e}_{a_i}$ is not truly an axial strain rate, the product $\dot{e}_{a_i} l$ (l = fiber length) gives the relative deflection of fiber ends and hence is a valid deformation measure.

Since fiber extensional strain rate depends only on the macroscopic membrane strain rates and the orientation of the fiber, θ_i, all fibers in the ith family have the same extensional strain rate. Since at collapse the deformation measures are those of the fiber limit state we have

$\dot{e}_{a_i} > 0$, fibers are deforming plastically or pulling out in tension, fiber load is their limit load in tension, f^0.

$\dot{e}_{a_i} < 0$, fibers are deforming plastically or buckling in compression, fiber load is their limit load in compression, $-\varphi_c f^0$.

$\dot{e}_{a_i} = 0$, fibers are not deforming, fiber load may be anywhere between limit loads in tension and compression, $-\varphi_c f^0 \leq f_i \leq f^0$.

Examining equation (8) it is seen that a linear velocity field gives the typical fiber strain rate shown in Fig. 3(a) as a function of θ. Within an orientation band of 2α, $\dot{e}_a$ is positive, and outside this band $\dot{e}_a$ is negative. Only at the two positions

$$\theta = \gamma \pm \alpha = \tan^{-1}[-\rho_1 \pm \sqrt{(\rho_1^2 - \rho_2)}] \tag{9}$$

where

$$\rho_1 = \frac{\dot{\varepsilon}_{xy}}{\dot{\varepsilon}_y}, \qquad \rho_2 = \frac{\dot{\varepsilon}_x}{\dot{\varepsilon}_y} \tag{10a, b}$$

is $\dot{e}_a$ zero, and a maximum of two fiber families are not undergoing limit deformation. Note that depending on the signs of ρ_1 and ρ_2, $\dot{e}_a$ may be negative inside and positive outside the 2α band.

The corresponding non-dimensional force in fibers as a function of θ is shown in Fig. 3(b). For the opposite case where $\dot{e}_a$ is negative inside the 2α band, $\varphi = -\varphi_c$ inside and $\varphi = 1$ outside the band.

Following the usual procedure for upper bound computation, the rates of work done by the external forces (N_x, N_y, N_{xy}) and by the internal forces (fiber forces f_i at the RSE boundary) are equated. The rate of external work, W, is given by

$$W = N_x \dot{\varepsilon}_x + N_y \dot{\varepsilon}_y + 2N_{xy} \dot{\varepsilon}_{xy}. \tag{11}$$

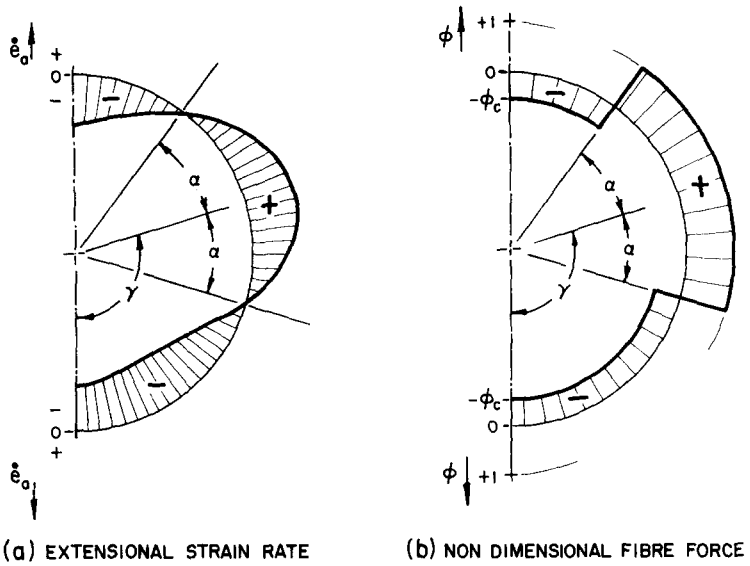

FIG. 3. Typical extensional strain rate and fiber force functions.

The rate of internal work, D, is

$$D = \sum_{\substack{\text{all}\\\text{fibers}}} \underset{\substack{\text{force}\\\text{in}\\\text{fiber}}}{f} \quad \underset{\substack{\text{relative}\\\text{motion of}\\\text{fiber ends}}}{\Delta l}$$

The relative motion of fiber ends may be written $\Delta l = \dot{e}_a l$ even in the case where fibers are buckling or pulling out, and hence from equation (8) we have

$$D = \dot{\varepsilon}_x \sum_{i=1}^{n} f_i v_i \cos^2\theta_i + \dot{\varepsilon}_y \sum_{i=1}^{n} f_i v_i \sin^2\theta_i + 2\dot{\varepsilon}_{xy} \sum_{i=1}^{n} f_i v_i \sin\theta_i \cos\theta_i. \tag{12}$$

It is noted that the rate of internal work D is uniquely determined by the assumed velocity field.

Setting $D = W$, we obtain

$$N_x\dot{\varepsilon}_x + N_y\dot{\varepsilon}_y + 2N_{xy}\dot{\varepsilon}_{xy} = \dot{\varepsilon}_x \sum_{i=1}^{n} f_i v_i \cos^2\theta_i + \dot{\varepsilon}_y \sum_{i=1}^{n} f_i v_i \sin^2\theta_i + 2\dot{\varepsilon}_{xy} \sum_{i=1}^{n} f_i v_i \sin\theta_i \cos\theta_i \tag{13}$$

Since $\dot{\varepsilon}_x$, $\dot{\varepsilon}_y$, and $\dot{\varepsilon}_{xy}$ are arbitrary, the equality must hold for their coefficients, and we recover the equilibrium equations (3a,b,c) with the f_i determined by their $\dot{e}_a$ as shown in Fig. 3(b). When applied to the n family membrane, this results in a fiber force system of

$$\begin{aligned} f_1 = f_2 = \cdots = f_{j-1} &= -\varphi_c f^\circ; \quad -\varphi_c f^\circ \le f_j \le +f^\circ \\ f_{j+1} = \cdots = f_{k-1} &= +f^\circ; \quad -\varphi_c f^\circ \le f_k \le +f^\circ \\ f_{k+1} = \cdots = f_n &= -\varphi_c f^\circ \end{aligned} \tag{14}$$

where j and k, $j < k$, pertain to the fiber families at the points where $\dot{e}_a = 0$, $j+1$ through $k-1$ are the families contained within the 2α band, and 1 through $j-1$ and $k+1$ through n

are the families outside the 2α band. Substituting (14) into the equilibrium equations, we obtain

$$
\begin{aligned}
N_x = & -\varphi_c f^\circ \sum_{i=1}^{j-1} v_i \cos^2\theta_i + f_j v_j \cos^2\theta_j + f^\circ \sum_{i=j+1}^{k-1} v_i \cos^2\theta_i \\
& + f_k v_k \cos^2\theta_k - \varphi_c f^\circ \sum_{i=k+1}^{n} v_i \cos^2\theta_i \\
N_y = & -\varphi_c f^\circ \sum_{i=1}^{j-1} v_i \sin^2\theta_i + f_j v_j \sin^2\theta_j + f^\circ \sum_{i=j+1}^{k-1} v_i \sin^2\theta_i \\
& + f_k v_k \sin^2\theta_k - \varphi_c f^\circ \sum_{i=k+1}^{n} v_i \sin^2\theta_i \\
N_{xy} = & -\varphi_c f^\circ \sum_{i=1}^{j-1} v_i \sin\theta_i \cos\theta_i + f_j v_j \sin\theta_j \cos\theta_j + f^\circ \sum_{i=j+1}^{k-1} v_i \sin\theta_i \cos\theta_i \\
& + f_k v_k \sin\theta_k \cos\theta_k - \varphi_c f^\circ \sum_{i=k+1}^{n} v_i \sin\theta_i \cos\theta_i
\end{aligned}
\tag{15a, b, c}
$$

where $-\varphi_c f^\circ \leq f_j, f_k \leq +f^\circ$. Equations (15) are linear functions of the two parameters f_j and f_k, and describe a bounded plane in three dimensional N_x, N_y, N_{xy} space in parametric form. This plane is an upper bound to a portion of the membrane limit surface. Replacing $+f^\circ$ with $-\varphi_c f^\circ$ in the above equations and vice-versa, an upper bound to another portion of the limit surface is obtained. Letting j and $k, j < k$, run through all possible combinations from 1 to n will yield a surface composed of $n!/(n-2)!$ flat faces which is an upper bound to the entire limit surface for the fibrous membrane.

To obtain a lower bound, merely assume the fiber force system (14) which resulted from the linear velocity field. It is seen that we recover equations (15) but this time as a lower bound to the limit surface. Since the upper and lower bounds coincide, it is concluded that equations (15) describe the true limit surface for the n family membrane element.

Hill [6] has proven that during plastic flow, the generalized strain rate vector associated with a generic point on the yield surface of a composite is normal to the yield surface at that point. Drucker [15, 16] has also shown that normality of the strain rate vector to the yield surface follows immediately if materials or structural elements obey the stability postulate. Since by definition we are considering fibers which behave in a neutrally stable way, normality is a direct consequence of our assumed material and structural behavior. However, normality can also be shown to follow directly from equations (7), (11) and (15).

The limit surface (15) is exact for the membranes considered; i.e. those whose fibers are held together by site bonds or impregnated with a strengthless matrix. The surface, however, is also a rigorous lower bound for structures whose fibers are imbedded in a perfectly plastic matrix whose strength is not negligible. This is readily seen by assuming a constant uniaxial stress in the fibers which varies with orientation in the manner of equation (14), and zero stresses in the matrix. By the lower bound theorem, the stress resultants (15) are lower bounds to the limit surface for a structure imbedded in a matrix of material which has an arbitrary limit condition. It is expected that the lower bound will be closer to the true limit surface as the strength and volume of matrix becomes smaller than the strength and volume of fibers.

In summary, for the general case of an n family fiber membrane composed of fibers which collapse by perfectly plastic flow, constant load buckling and constant load pullout, introduction of a fiber force field of the form (14) into the equilibrium equations (3) will give an $n!/(n-2)!$ faced limit surface in N_x, N_y, N_{xy} space which is exact for site bonding or strengthless matrices and a lower bound for matrices having nonzero strength. In order to compute the limit surface for a particular membrane, the orientation, number density and tensile and compressive limit loads of the fibers which compose it must be known.

As examples of use of the above theory and to illustrate some effects of fiber orientation, we will compute limit surfaces for membrane configurations shown in Fig. 4. For simplicity, assume that the fiber limit loads are equal in tension and compression giving $\varphi_c = 1$.

Case (a) [*Fig. 4(a)*]. Three families having equal fiber density $v_1 = v_2 = v_3 = v^0/3$ but oriented at $-45°$, $0°$ and $+45°$ with the x axis. The length of fibers per unit area, L_f, and mass per unit area, M_f, are equal to v^0 and $\rho_l v^0$, respectively. Equilibrium in non-dimensional form is

$$n_x = \frac{\varphi_1}{6} + \frac{\varphi_2}{3} + \frac{\varphi_3}{6}; \qquad n_y = \frac{\varphi_1}{6} + \frac{\varphi_3}{6}; \qquad n_{xy} = \frac{\varphi_3}{6} - \frac{\varphi_1}{6} \tag{16}$$

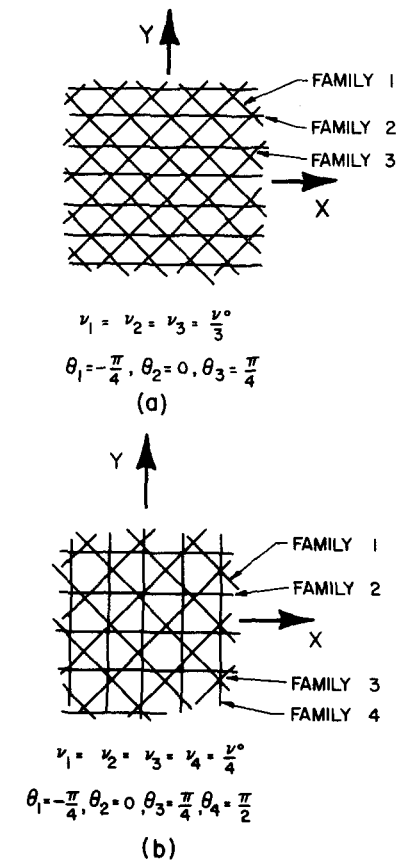

FIG. 4. Fiber membranes with different fiber orientation, but the same total number of fibers.

All combinations of type (14) are given non-dimensionally as follows:

$$-1 \le \varphi_1 \le 1, \qquad \varphi_2 = \pm 1, \qquad -1 \le \varphi_3 \le 1 \tag{17a}$$

$$-1 \le \varphi_1 \le 1, \qquad -1 \le \varphi_2 \le 1, \qquad \varphi_3 = \pm 1 \tag{17b}$$

$$\varphi_1 = \pm 1, \qquad -1 \le \varphi_2 \le 1, \qquad -1 \le \varphi_3 \le 1 \tag{17c}$$

which, when substituted in the equilibrium equations, yield the following six bounded planes shown in Fig. 5(a):

$$\left.\begin{aligned} n_x &= \varphi_1/6 + \varphi_3/6 \pm \tfrac{1}{3} \\ n_y &= \varphi_1/6 + \varphi_3/6, \qquad -1 \le \varphi_1, \varphi_3 \le 1 \\ n_{xy} &= \varphi_3/6 - \varphi_1/6 \end{aligned}\right\} \tag{18a}$$

$$\left.\begin{aligned} n_x &= \varphi_1/6 + \varphi_2/3 \pm \tfrac{1}{6} \\ n_y &= \varphi_1/6 \pm \tfrac{1}{6}, \qquad -1 \le \varphi_1, \varphi_2 \le 1 \\ n_{xy} &= \pm \tfrac{1}{6} - \varphi_1/6 \end{aligned}\right\} \tag{18b}$$

$$\left.\begin{aligned} n_x &= \pm \tfrac{1}{6} + \varphi_2/3 + \varphi_3/6 \\ n_y &= \pm \tfrac{1}{6} + \varphi_3/6, \qquad -1 \le \varphi_2, \varphi_3 \le 1 \\ n_{xy} &= \varphi_3/6 \mp \tfrac{1}{6} \end{aligned}\right\} \tag{18c}$$

Case (b) [*Fig. 4(b)*]. Four families having equal fiber density $v_1 = v_2 = v_3 = v_4 = v^0/4$ oriented at $-45°$, $0°$, $+45°$ and $+90°$ with the x axis. The total length per unit area of fibers is still v^0. In an identical manner to case (a), substituting all possible force combinations obtainable from (14) into equilibrium equations from (6), we get the twelve sided limit surface shown in Fig. 5(b). Note that the four family membrane has greater load bearing capacity in uniaxial tension but less in pure shear than the three family membrane for the choice of axes shown.

Continuous fiber distribution

A membrane composed of n fiber families has an exact limit surface containing $n!/(n-2)!$ flat faces. As n gets very large it will be cumbersome to perform computations using the exact limit criteria and it will be convenient to develop a continuous approximation to this surface.

Let it be assumed that the fibers in the ith family are spread uniformly between θ_i and θ_{i+1} instead of being oriented at θ_i.

Define the number of fibers per unit length per unit angle oriented at $\theta_i + \Delta\theta_i/2$ as

$$\bar{v}_i = \frac{v_i}{\Delta\theta_i} \tag{19}$$

where

$$\left.\begin{aligned} \Delta\theta_i &\equiv \theta_{i+1} - \theta_i, \qquad i \ne n \\ \Delta\theta_n &\equiv \theta_1 + \pi/2 - \theta_n, \qquad i = n \end{aligned}\right\} \tag{20}$$

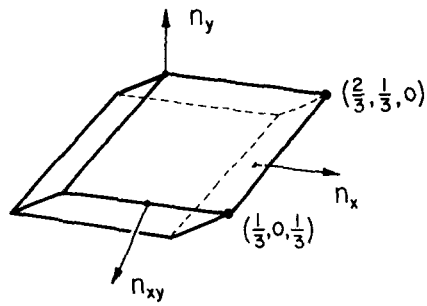

(a)

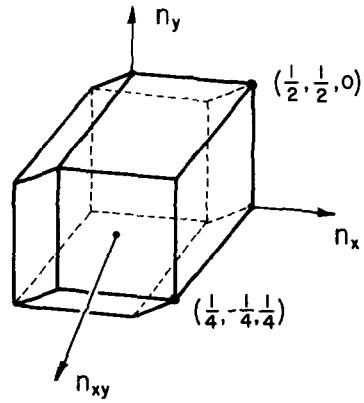

(b)

FIG. 5. (a) Limit surface for membrane shown in Fig. 4(a). (b) Limit surface for membrane shown in Fig. 4(b).

An approximation of $\bar{v}_i$ as n gets large and $\Delta\theta_i$ gets small is to draw a smooth curve $v(\theta)$ through $\bar{v}_i$. The equilibrium equations in terms of the continuous function $v(\theta)$ can be written

$$N_x = \int_{-\pi/2}^{\pi/2} f(\theta)v(\theta)\cos^2\theta \, d\theta \tag{21a}$$

$$N_y = \int_{-\pi/2}^{\pi/2} f(\theta)v(\theta)\sin^2\theta \, d\theta \tag{21b}$$

$$N_{xy} = \int_{-\pi/2}^{\pi/2} f(\theta)v(\theta)\sin\theta\cos\theta \, d\theta \tag{21c}$$

These equations with $v(\theta)$ known and $f(\theta)$ given non-dimensionally by Fig. 3(b) are an approximation to the limit surface in terms of the angle parameters γ and α:

$$N_x = -\varphi_c f^\circ \int_{-\pi/2}^{-\pi/2+\gamma-\alpha} v(\theta)\cos^2\theta\,d\theta + f^\circ \int_{-\pi/2+\gamma+\alpha}^{-\pi/2+\gamma+\alpha} v(\theta)\cos^2\theta\,d\theta - \varphi_c f^\circ \times \int_{-\pi/2+\gamma+\alpha}^{\pi/2} v(\theta)\cos^2\theta\,d\theta \tag{22a}$$

$$N_y = -\varphi_c f^\circ \int_{-\pi/2}^{-\pi/2+\gamma-\alpha} v(\theta)\sin^2\theta\,d\theta + f^\circ \int_{-\pi/2+\gamma-\alpha}^{-\pi/2+\gamma+\alpha} v(\theta)\sin^2\theta\,d\theta - \varphi_c f^\circ \times \int_{-\pi/2+\gamma+\alpha}^{\pi/2} v(\theta)\sin^2\theta\,d\theta \tag{22b}$$

$$N_{xy} = -\varphi_c f^\circ \int_{-\pi/2}^{-\pi/2+\gamma-\alpha} v(\theta)\sin\theta\cos\theta\,d\theta + f^\circ \int_{-\pi/2+\gamma-\alpha}^{-\pi/2+\gamma+\alpha} v(\theta)\sin\theta\cos\theta\,d\theta - \varphi_c f^\circ \int_{-\pi/2+\gamma+\alpha}^{\pi/2} v(\theta)\sin\theta\cos\theta\,d\theta \tag{22c}$$

The mechanics of fiber membrane structures divides rather neatly, then, into two main areas: those fiber membranes containing many fiber families where a continuous function $v(\theta)$ may be used without serious error, and those membranes where the discrete formulation must be used to maintain accuracy. It is remarked that if the relation

$$v(\theta) = \sum_{i=1}^{n} v_i \delta(\theta - \theta_i) \tag{23}$$

where $\delta(\theta-\theta_i)$ is the Dirac impulse function, is substituted into (21a, b, c), the exact equilibrium equations (3) are recovered. One may therefore equally well use the equations for continuous fiber orientation distribution (21a, b, c) with the fiber force function in Fig. 3(b) and the relation (23) and still retain complete accuracy and generality.

A comparison between continuous and discrete formulations gives

$$\int_{-\pi/2}^{\pi/2} v(\theta)\,d\theta = \sum_{i=1}^{n} v_i \tag{24}$$

and hence the length and mass density functions (1) and (2) become for the continuous case,

$$L_f = \int_{-\pi/2}^{\pi/2} v(\theta)\,d\theta \tag{25}$$

$$M_f = \rho_l \int_{-\pi/2}^{\pi/2} v(\theta)\,d\theta. \tag{26}$$

As an example, consider a membrane composed of many fibers uniformly distributed from $\theta = -\pi/2$ to $+\pi/2$ such that $v(\theta) = v^c = \text{const}$. Here, v^c is not the total length of fibers per unit membrane area, but is related to it by equation (25):

$$L_f = \pi v^c.$$

The membrane is then isotropic. Let, also, the fiber limit loads be equal in tension and compression so that $\varphi_c = 1$. Substituting for ν and φ_c in (21a, b, c), non-dimensionalizing in the manner of (6a, b, c), integrating and simplifying,

$$n_x = \frac{2\alpha}{\pi} - \frac{1}{2} - \frac{1}{\pi}\sin 2\alpha \cos 2\gamma$$

$$n_y = \frac{2\alpha}{\pi} - \frac{1}{2} + \frac{1}{\pi}\sin 2\alpha \cos 2\gamma \qquad (27a, b, c)$$

$$n_{xy} = \frac{-1}{\pi}\sin 2\alpha \sin 2\gamma$$

$$\text{where } 0 \leq \alpha+\gamma \leq \pi, \alpha \leq \gamma$$

Eliminating γ and α, the limit surface equation becomes

$$\left[\frac{\pi}{2}(n_x - n_y)\right]^2 - [\pi n_{xy}]^2 = \cos^2\left[\frac{\pi}{2}(n_x + n_y)\right]. \qquad (28)$$

This surface is shown in Fig. 6. Note that for isotropic plastic materials in plane stress the surface (28) resembles both the Tresca yield surface (ellipsoidal cylinder capped by two right elliptical cones) and the von Mises ellipsoid. Furthermore, it is also interesting to note that for $n_{xy} = 0$, the isotropic fibrous limit surface becomes two intersecting cosine curves and resembles closely a yield condition proposed by von Mises [17] composed of two intersecting parabolae.

Unequal fiber tensile and compressive limit loads—fiber buckling and pullout

As discussed earlier, fiber buckling and pullout are possible limit phenomena especially when no matrix material surrounds the fibers. There is also evidence to suggest that some fibers have unequal tensile and compressive yield strengths [18]. All these phenomena will result in $\varphi_c \neq 1$, the exact value of φ_c to be determined by the particular limit mechanisms involved.

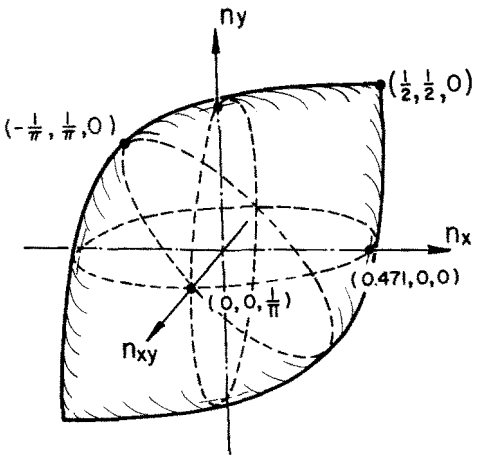

FIG. 6. Limit surface for uniform, continuous fiber orientation distribution.

The qualitative effect of $\varphi_c \neq 1$ can be seen by rewriting the general limit surface equations (15) or (22) as

$$N_x = \left(\frac{1+\varphi_c}{2}\right)N_x^1 + \left(\frac{1-\varphi_c}{2}\right)N_x^\circ$$

$$N_y = \left(\frac{1+\varphi_c}{2}\right)N_y^1 + \left(\frac{1-\varphi_c}{2}\right)N_y^\circ \qquad (29a, b, c)$$

$$N_{xy} = \left(\frac{1+\varphi_c}{2}\right)N_{xy}^1 + \left(\frac{1-\varphi_c}{2}\right)N_{xy}^\circ$$

where N_x^1, N_y^1 and N_{xy}^1 are values on the limit surface for $\varphi_c = 1$; N_x° and N_y° are the values of N_x and N_y, respectively, when all fibers are collapsing in tension and are therefore the maximum positive normal membrane forces; and N_{xy}° is the value of N_{xy} when $N_x = N_x^\circ$ and $N_y = N_y^\circ$. Hence, determining the limit surface for $\varphi_c \neq 1$ from the limit surface for $\varphi_c = 1$ can be interpreted geometrically as holding the point $(N_x^\circ, N_y^\circ, N_{xy}^\circ)$ stationary in N_x, N_y, N_{xy} space and shrinking ($\varphi_c < 1$) or expanding ($\varphi_c > 1$) all linear dimensions to $(1+\varphi_c)/2$ times what they originally were (Fig. 7).

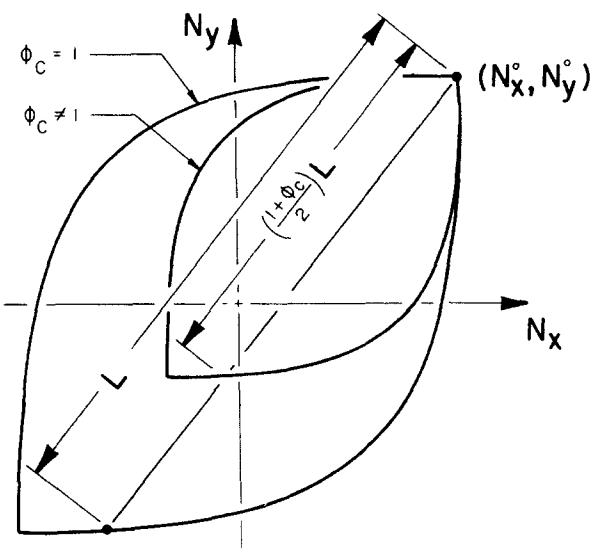

Fig. 7. Effect of unequal tensile and compressive limit loads for fibers.

To illustrate fiber buckling, consider the three family fiber membrane analyzed previously for fiber limit loads equal in tension and compression. Suppose the fibers are extremely thin and not embedded in a matrix, and the distance between fiber crossings is large so that the fibers buckle under an infinitesimal compressive load ($\varphi_c = 0$). A comparison between load bearing capacity of the same membrane with and without a matrix to prevent buckling is shown in Fig. 8(a). Note that the surface with fiber buckling cannot carry the same variety of loading as can the surface without buckling. For example, no compressive normal membrane force is allowed.

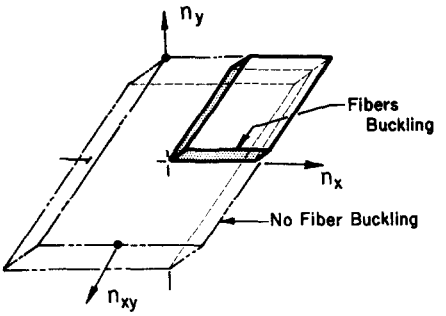

(a) FIBERS BUCKLING AT ZERO COMPRESSIVE LOAD

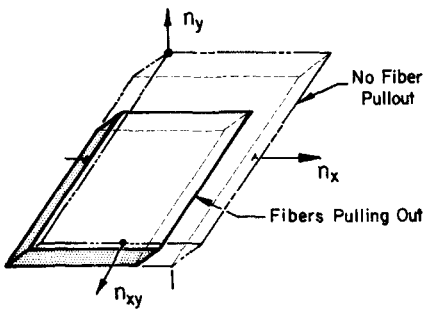

(b) FIBERS PULLING OUT AT HALF THEIR PLASTIC YIELD LOAD

FIG. 8. Limit surfaces for three family fiber membrane showing fiber buckling and pullout.

An illustration of fiber pullout in tension is given by the same three family membrane with fibers pulling out of the structure at a tensile load of $f^\circ/2$. The resulting limit surface is shown in Fig. 8(b). As one would expect, this particular fiber pullout load greatly reduces the tensile load bearing capacity of the membrane.

COMPARISON WITH EXPERIMENTAL DATA

Uniaxial tensile tests of thick, planar isotropic mats of metal fibers by the Huyck Corporation are described in [19], where the fiber plastic limit load in tension is known. As will be seen, it is possible to predict an upper bound to the ultimate uniaxial tensile strength of the mat. Also, tensile tests of several anisotropic nonwoven fabrics which were reported by Cusick, *et al.* [20] and Hearle and Stevenson [14], give ultimate uniaxial tensile strength as a function of the angle to the fabrics' cross-machine direction at which the samples were cut. Even though the absolute tensile strength values cannot be predicted because the fiber limit loads are not known, the shapes of analytical and experimental tensile strength vs. sample angle curves can be compared.

The mechanical properties of *Fibermetal*, a sintered metal fiber mat manufactured by the Huyck Metals Company for accoustic, filtration and composite materials applications, are presented in Ref. [19]. Mats for which both fiber tensile limit load and mat uniaxial tensile limit load are available were made from lengths of 347 stainless steel wire, 0·002 and 0·004 in. diameter, respectively, the wires having an ultimate tensile strength of about

100,000 psi. The wire lengths were made into mats with approximately uniform planar orientation distributions, but different apparent densities by a sintering process which site-bonded the fibers at their crossings.

For an isotropic fiber mat which collapses by plastic flow of fibers in tension and compression, the limit surface is given by equations (6) and (28). If we let the direction of pull be the x direction, then for uniaxial tension, $N_y = N_{xy} = 0$. Equations (6) and (28) then give

$$N_x = 0{\cdot}47\pi f^\circ v^\circ. \tag{30}$$

Now, the nominal mat stress is given by the tensile force per unit width, N_x, divided by specimen thickness, t, and can be written from equation (30) as

$$N_x/t = 0{\cdot}47\sigma^\circ A_f L_f/t \tag{31}$$

where A_f is the fiber cross sectional area and $L_f = \pi v^\circ$ is the fiber length density. In terms of the mat density in units of percentage of solid metal, D, we get for $\sigma^\circ = 100{,}000$ psi.

$$N_x/t = 470\, D\,(\%)\ \text{psi} \tag{32}$$

for prediction of ultimate tensile mat strength if all fibers fail plastically.

It was observed [19] that mat failure was caused primarily by failure at interfiber bonds for low densities, but more by failure of individual fibers at higher densities. The bond failure mode was noticed more markedly for the 0·004 in. diameter wire mats than for the 0·002 in. diameter wire mats. In addition, there may be fibers buckling in compression at the low mat densities which at the higher densities fail plastically in compression due to greatly decreased unsupported length.

Since fibers cannot develop their full plastic limit load because of bond failure and possibly buckling, equation (32) is not expected to agree with test data at low densities. Because the larger diameter fiber mats showed more marked bond failure, it is expected that their strengths will be less than for the thin diameter fiber mats. In all cases, (32) should be an upper bound to mat ultimate tensile strengths since fiber buckling and bond failure, if they occur, will take place at a stress lower than or equal to the fiber tensile yield stress.

Experimental results of nominal mat ultimate stress versus mat density from [19] are plotted in Fig. 9 along with the upper bound (32). As predicted, test data are not near the upper bound for low densities, but come to within 96 and 72 per cent of the upper bound at the highest densities tested for the 0·002 and 0·004 in. diameter wire mats, respectively. At all densities, the smaller diameter wire mats exhibit the higher ultimate strength as expected.

Hearle and Stevenson [14] report uniaxial tensile tests of samples of three different anisotropic non-woven fabrics where fiber orientation distributions have been determined. Of the three fabrics, only the Lantor, Ltd. 5206.L non-woven made from viscose fibers bonded with an acrylic binder is known to fail by pullout of fibers from the remainder of the web.

A typical membrane force (force/unit length) vs. membrane strain curve from [20] for the 5206.L fabric shows a large area before failure where strain can increase with essentially no increase in membrane force. It seems reasonable, therefore, to assume that the fibers are pulling out under constant load.

Uniaxial tensile tests were performed on samples cut at various angles θ to the non-wovens' cross-machine direction (the cross-machine direction is arbitrarily chosen as the x-axis and corresponds to $\theta = 0$). To obtain a prediction of fabric strength as a function

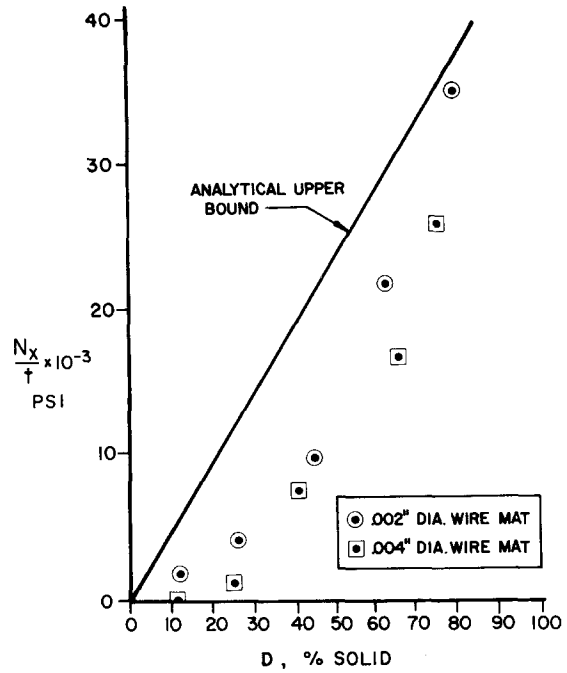

FIG. 9. Experimental and analytical 347 S.S. wire mat nominal ultimate tensile strength vs. mat density. Experimental values from [19].

of sample angle, let n_x, n_y, n_{xy} be the non-dimensional membrane stresses for x–y axis imbedded in the fabric. It is required that non-dimensional uniaxial tensile stress t in the x' direction be the only non-zero membrane stress in the x'–y' coordinate system at an angle θ with the original x–y axes. This, in turn, requires that

$$t(\theta) = n_x + n_y$$
$$\tan\theta = n_y/n_x \qquad (33a, b, c)$$
$$n_{xy}^2 - n_x n_y = 0$$

Therefore, values on the limit surface of a non-woven which satisfy equation (33c) correspond to the ultimate tensile strength t of a sample cut at an angle θ with the machine direction given by (33a, b).

To compute the limit surfaces of the non-woven fabric, it was assumed that fiber limit strengths were equal in tension and compression, and equations (22a, b, c) were numerically integrated on a digital computer using the experimentally determined values of fiber orientation distribution [Fig. 10(a)]. The computer program included a Newton–Raphson iteration technique to find values of n_x, n_y on the limit surface where equation (33c) is satisfied, and computed the corresponding values of t and θ.

Both analytical and experimental results are shown in Fig. 10(b). Since the actual fiber limit load is not known, the scales of the analytical and experimental values were adjusted to coincide at $\theta = \pi/2$. It is seen that good agreement between predicted and experimental values is obtained.

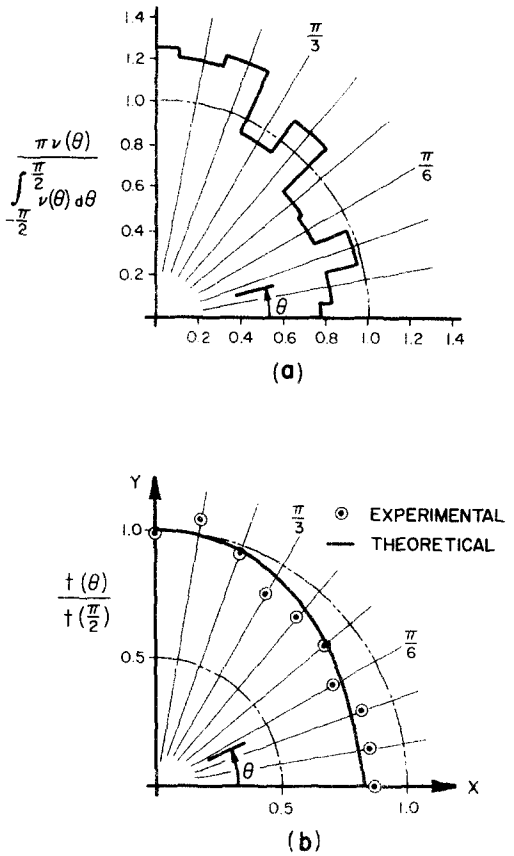

FIG. 10. (a) Fiber orientation distribution from [14]. (b) Comparison of theoretical and experimental [14] ultimate tensile strength vs. sample orientation angle. Lantor Ltd. 5206.L Fabric.

CONCLUSIONS

Load bearing capacity of fibrous membranes in the form of limit surfaces can be computed from methods and equations presented herein. Fibers which are site bonded to form a structure as well as those imbedded in an essentially strengthless matrix can be treated as long as exhaustion of additional load bearing capacity occurs for any combination of the following three reasons:

(1) perfectly plastic flow of fibers,
(2) constant load elastic buckling of fibers,
(3) pullout of fibers under constant load from the remaining structure.

The limit mechanism and fiber limit loads must be known for the particular fibrous structure under consideration.

The limit surfaces derived herein also represent rigorous lower bounds to a fibrous composite structure containing a perfectly plastic matrix material whose strength is not negligible. It is expected that this lower bound will be close to the true limit surface for structures where matrix strength and volume are small compared to fiber strength and volume.

The complete generality of the limit surface equations in terms of the fiber orientation density makes them particularly valuable for analyzing ultimate strength characteristics of fibrous membranes. A degree of complexity has been removed since the basic structural material is no longer the fibers, but the structural element having limit characteristics computed from the preceding equations. In addition, the equations make it possible for the design engineer to evaluate structural designs having different fiber orientation densities, and hence obtain optimal configurations for particular applications.

Available experimental data indicate reasonable agreement with theory for those materials that are known to exhibit acceptable limit behavior.

REFERENCES

[1] B. W. ROSEN, Mechanics of composite strengthening. *Fiber Composite Materials*. American Society for Metals (1964).

[2] M. A. SADOWSKY, S. L. PU and M. A. HUSSAIN, Buckling of microfibers. *J. appl. Mech.* **34**, 1011–1016 (1966).

[3] J. W. S. HEARLE and P. J. STEVENSON, Nonwoven fabric studies—IV. Prediction of tensile properties. *Textile Res. J.* **34**, 181–191 (1964).

[4] P. V. MCLAUGHLIN, Jr. and S. C. BATTERMAN, On extending the range of applicability of the limit theorems. *J. appl. Mech.* in press.

[5] D. C. DRUCKER, W. PRAGER and H. J. GREENBERG, Extended limit design theorems for continuous media. *Q. appl. Math.* **9**, 381–389 (1952).

[6] R. HILL, The essential structure of constitutive laws for metal composites and polycrystals. *J. Mech. Phys. Solids* **15**, 79–95 (1967).

[7] D. C. DRUCKER, Engineering and continuum aspects of high strength materials. High strength materials. *Proc. 2nd Berkeley Int. Mater. Conf.*, p. 795, edited by V. F. ZACKEY. Wiley (1965).

[8] Z. HASHIN, Transverse strength of fibrous composites. Evaluation of Filament-Reinforced Composites for Aerospace Structural Applications. NASA CR-207 (1965).

[9] L. S. SHU and B. W. ROSEN, Strength of fiber-reinforced composites by limit analysis methods. *J. comp. Mater.* **1**, 366–381 (1967).

[10] N. F. DOW, B. W. ROSEN, L. S. SHU and C. H. ZWEBEN, Design Criteria and Concepts for Fibrous Composite Structures. Final Report for NASA contract NASw-1377 (1967).

[11] G. GERARD and C. LASHMIKANTHAM, Structural Design Synthesis Approach to Filamentary Composites. NASA CR-964 (1967).

[12] B. W. SHAFFER, Elastic-plastic stress distribution within reinforced plastics loaded normal to its internal filaments. *AIAA Jnl* **6**, 2316–2324 (1968).

[13] J. F. MULHERN, T. G. ROGERS and A. J. M. SPENCER, A continuum theory of a plastic-elastic fibre-reinforced material. *Int. J. Engng Sci.* **7**, 129–152 (1969).

[14] J. W. S. HEARLE and P. J. STEVENSON, Nonwoven fabric studies—III. The anisotropy of nonwoven fabrics. *Textile Res. J.* **33**, 877–888 (1963).

[15] D. C. DRUCKER, On the postulate of stability of materials in the mechanics of continua. *J. Méc.* **3**, 235–249 (1964).

[16] D. C. DRUCKER, Plasticity. In *Structural Mechanics*, pp. 407–455, edited by J. N. GOODIER and N. J. HOFF. Pergamon Press (1960).

[17] R. VON MISES, Three remarks on the theory of the ideal plastic body. *Reissner Anniversary Volume*, pp. 415–429, edited by Staff of Department of Aero. Engng and Mech. Engng of Polytechnic Institute, Brooklyn. Edwards (1949).

[18] W. BOBETH, *et al. Faserforsch. u. Textiltech.* **18**, 547–553 (1967); Abstracted in *Textile Tech. Dig.* **25**, Abstract No. 4165 (1968).

[19] J. J. CIMEROL, A. R. ERICKSON and J. J. FISHER, Investigation of the Properties of Fibermetal Acoustical Materials. NASA CR-66643 (1968).

[20] G. E. CUSICK, J. W. S. HEARLE, R. I. C. MICHIE, R. H. PETERS and P. J. STEVENSON, Physical properties of some commercial non-woven fabrics. *J. Textile Inst. Proc.* **54**, 52–74 (1963).

(*Received* 24 *July* 1969; *revised* 8 *December* 1969)

Абстракт—В работе исследуется предельное поведение волокнистых материалов, составленных из плоских рядов длинных, упругих, идеально пластических волокон, связанных в узлах или расположен ных в ненапряженной решетке. Используются теоремы предельного верхнего и инжнего ограничения для получения уравнений предельных поверхностей представленных элементов конструкции волокнистых мембран, выраженных числом, направлением и предельной нагрузкой составляющих волокон. В теории даются эффекты геометрии направления волокон, их течение, выпучивание и удаление из остальной конструкции. Все это иллюстрируется численными примерами. Экспериментальные результаты, касающиеся опытов на растяжение металлических проволочных сеток и неплетенных тканей сравниваются с аналитическими предположениями.